Journal of Arid Environments 198 (2022) 104695

Contents lists available at ScienceDirect

Journal of Arid Environments

journal homepage: www.elsevier.com/locate/jaridenv

El Niño Southern Oscillation and enhanced arid land vegetation productivity in NW South America

Benjamin R. Vining [a,*], Aubrey Hillman [b], Daniel A. Contreras [c]

[a] Environmental Dynamics and Department of Anthropology, 330 Old Main, University of Arkansas-Fayetteville, Fayetteville, AR, 72701, USA
[b] Department of Atmospheric and Environmental Sciences, University at Albany, State University of New York, Albany, NY, 12222,, USA
[c] Department of Anthropology, Turlington Hall, University of Florida, Gainesville, FL, 32603, USA

ARTICLE INFO

Keywords:
Remote sensing
Sentinel 2
Gross primary productivity
Vegetation time series
el Niño-Southern oscillation
ENSO
Terrestrial ecology
Desert vegetation biomes
NW South America

ABSTRACT

El Niño Southern Oscillation (ENSO) is a periodic disruption of coupled oceanic-atmospheric conditions in the tropical Pacific, which changes global precipitation regimes. One area strongly affected by positive (el Niño) phases is the Pacific Coast of South America. The specific effects of ENSO on Andean ecological communities have received little attention, however. We examine vegetation gross primary productivity (GPP) on Peru's north coast arid-lands during a recent (2016–2017) el Niño, using a time series of Sentinel 2 imagery. By comparing GPP time-series in three agricultural subregions and three endemic desert vegetation communities, we demonstrate that levels of primary productivity in desert regions during ENSO-positive phases meet or exceed thresholds of adjacent agricultural lands. These results, the first that quantify and spatialize changing GPP between ENSO-neutral and ENSO-positive phases for South American arid-land biomes, both outline the scale and distribution of the el Niño effects on terrestrial ecosystems and highlight the resulting opportunities for human inhabitants. The dramatic changes to endemic vegetation on the normally hyperarid coastal desert of Peru revealed by reconstructed GPP suggest that periodic el Niño precipitation plays a critical role in arid land ecodynamics by enhancing establishment, green growth, and seedbank development. These findings improve our understanding of ENSO's net effects and highlight the roles of abrupt climate events in the arid land ecology of NW South America.

1. Introduction

South America's Pacific coast, between approximately 4°–30° S latitude, is one of the most extensive coastal deserts globally. This region is affected by the El Niño Southern Oscillation (ENSO), a periodic disruption of coupled oceanic-atmospheric conditions originating in the tropical Pacific. ENSO events generally are differentiated from normal or ENSO-neutral conditions as ENSO-positive (warm, or 'el Niño') and ENSO-negative (cool, or 'la Niña') phases, which bring wetter or drier seasons, respectively, to South America's desert coast. Research into the ecological and societal impacts of ENSO in this region has emphasized the adverse effects of ENSO-positive (el Niño) events, especially economic losses in marine fisheries from warming oceans and nutrient deprivation (Castilla and Camus, 1992; Chavez et al., 2003; Kluger et al., 2018; Ñiquen and Bouchon, 2004) and losses to transportation, agricultural, and sanitation infrastructure from flooding and river avulsions (Garnica, 1997; Martinez-Urtaza et al., 2008; Ward et al., 2014).

ENSO's effects on South America's arid coastal environments remain poorly understood even though this is a core region of ENSO development. ENSO has been hypothesized to be a key factor in the formation of arid-adapted endemic vegetation communities (Cano et al., 1999; Eichler and Londoño, 2013; Tovar et al., 2018). Botanical surveys following strong el Niños in 1982–1983 and 1997–1998 suggest endemic vegetation communities in the Andean desert are at least partially adapted to the semi-regular, periodic ENSO climatic pattern, and may rely on el Niño events for their ecological function (Cano et al., 1999; Dillon and Rundel, 1990; Eichler and Londoño, 2013; Péfaur, 1982; Richter, 2005; Tovar et al., 2018). Human usage of these arid environs may also, in long-term perspective, be ENSO-adapted. Although early use of desert areas has been tied to early – mid Holocene pluvial phases (e.g., Chauchat, 1975), more recent studies suggest desert environments could have been utilized intermittently during ENSO-positive periods when increased precipitation enhanced their productive potentials (Beresford-Jones et al., 2015; Caramanica et al.,

* Corresponding author.
E-mail address: vining@uark.edu (B.R. Vining).

https://doi.org/10.1016/j.jaridenv.2021.104695
Received 27 April 2021; Received in revised form 11 October 2021; Accepted 25 November 2021
Available online 2 December 2021

2020; Gálvez Mora and Runcio, 2010).

These divergent perspectives have led to a heightening debate regarding the net ecological effects of ENSO-positive phases on marine and terrestrial productivity, and ultimately the adaptive capacity of human communities to shift productive strategies to adjust to abrupt ENSO climate shifts.

In the context of this debate, we examine changing vegetation Gross Primary Productivity (GPP) on the north coast of Peru during a recent (2016–2018) cycle between ENSO-neutral and ENSO-positive conditions. Our objective is to assess the productive potential of desert microenvironments with respect to human exploitation (either through animal husbandry, foraging or small-scale cultivation) and whether potential niches that develop during el Niño events could offset other, adverse impacts of these events. To do so, we quantify and spatialize ENSO-driven trends in GPP using a time-series of Sentinel 2 multispectral satellite data. Our estimates of GPP are validated by establishing their strong correlation with Moderate Resolution Spectroradiometer (MODIS) GPP products. To evaluate how vegetation responses in endemic communities compares to various production strategies, we compare GPP in three desert phytogeographic zones to three adjacent agricultural subregions at high spatial and moderate temporal resolution. This approach allows us to characterize changes in ecological potentials and identify areas where climatic microrefugia may develop.

We find that GPP in select endemic vegetation communities increases rapidly to levels commensurate with those in agricultural areas and is sustained for several months. These often-overlooked consequences of el Niño are key to understanding the ecological role and net effects of this climatic pattern. Understanding the spatio-temporal responses of endemic dryland vegetation GPP to ENSO dynamics is an essential step towards appreciating the net effects of this climatic pattern on terrestrial ecology.

2. Geographic and climatic context

2.1. Study region

We focus our analysis on endemic desert vegetation communities surrounding Peru's lower Chicama and Jequetepeque Valleys (7.6°–8.0° S, 79.0°–79.5° W, 0–2100 masl, Fig. 1A and B). In this region, significant vegetation (and by extension major habitats and human land use) is confined to riparian 'oases' along rivers draining the Andean chain, while surrounding lands are warm and hyperarid. Higher-elevation fog oases are an important but highly localized secondary vegetation community (Moat et al., 2021). Outside of these limited vegetation zones, desert areas are largely denudate under normal climatic conditions.

Mean annual temperature is 21.2 °C with seasonal/diurnal variations ±11 °C. Surface and groundwater originates as high-elevation orographic precipitation from Atlantic-Amazonian convective sources (Vuille et al., 2000). Precipitation occurs as small events of <5 mm during the austral wet season (December–May), with most accumulation occurring between late February–April. During ENSO-neutral years, mean precipitation recorded at the *Servicio Nacional de Meteorología e Hidrología* (SENAMHI) instrumental stations at Casa Grande (−7.75°, −79.19°, 145 masl) and San Benito (−7.42°, −78.92°, 1317 masl) are 21.46 mm/annum and 322.47 mm/annum, respectively (SENAMHI, 2019).

The various phytogeographic zones of the study region, differentiated by elevation, geological substrate, and mean ambient moisture, allow us to evaluate the effects of changing moisture regimes on vegetation productivity in distinct environmental settings across ENSO phases (Fig. 1C). The lower Chicama Valley is a deltaic alluvial plain, approximately 70% of which is currently under intensive fertigated sugarcane (*Saccharum* sp.) monoculture. The lower Jequetepeque Valley, in the northern portion of the study region, is largely covered in sugarcane and rice (*Oryza* sp.) monoculture. Small-scale monoculture and polyculture plots are concentrated in the NW portion of the Chicama Valley, predominantly over marginal solonchak soils and are interspersed with remnant endemic thorn-scrub, halophytic grasses, and back-coastal marshlands.

The desert areas surrounding these alluvial plains are divided into three phytogeographic subregions (ONERN, 1973). The desert littoral (0–200 masl) is a region of sparse xerophytic grasses and terrestrial epiphytes (*Tillandsia* sp.) growing over aeolian sands and paleochannel deposits. The desert piedmont is a narrow transitional band between 200

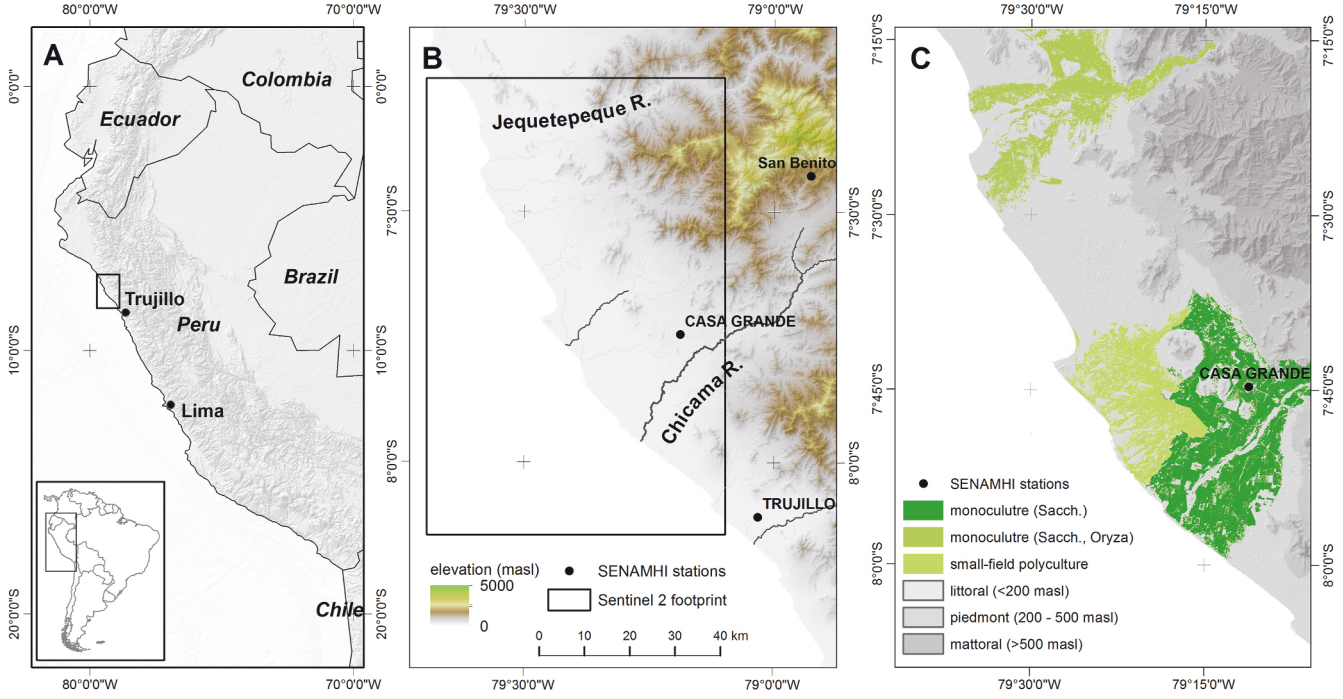

Fig. 1. (A) The location of the study area in NW South America. (B) The Chicama and Jequetepeque Valleys, with the Sentinel 2 imagery footprint (black outline) and SENAMHI meteorological stations indicated. (C) Phytogeographic subregions in the study area.

and 500 masl characterized by alluvial fan deposits, poorly formed regosols, and sparse xerophytic vegetation. The desert matorral region is found from approximately 500–2000 masl, is associated with xerosols and leptosols, and hosts succulent, and sparse thorn-scrub where pockets of moisture allow. We evaluate the effects of ENSO-driven precipitation, such as that which occurred during the most recent 2016–2017 el Niño, on GPP these agricultural and endemic phytogeographic communities.

2.2. ENSO characteristics within the study region

El Niño-Southern Oscillation (ENSO) is a periodic disruption of coupled oceanic-atmospheric circulation patterns originating in the tropical Pacific Ocean (Fig. 2), which create sea surface temperature and precipitation anomalies that change local and global climates. ENSO is characterized by two phases representing departures from interannual mean (ENSO-neutral) conditions; an ENSO-positive (warm or "el Niño") phase and an ENSO-negative (cool or "la Niña") phase. A variety of ENSO patterns are currently recognized based on whether SSTA develop in the Eastern Pacific (EP, NINO 1 + 2) or Central Pacific (CP, NINO 3, 3.4, and 4) and how these affect moisture balance in adjacent regions (Ashok et al., 2007; Cai et al., 2020; Chattopadhyay et al., 2019; Hu et al., 2019; Ramírez and Briones, 2017, see Fig. 2).

The frequency and magnitude of ENSO phases are modulated by their spatio-temporal intersection with other interannual – decadal oceanic-atmospheric oscillations, including the Pacific Decadal Oscillation and Atlantic Multidecadal Oscillation (Chattopadhyay et al., 2019; Ramírez and Briones, 2017). Shifts from ENSO-neutral to positive/negative phases develop over approximately 7–12 months and occur on cycles of 3–7 years. Strong positive/negative phases occur with decadal periodicity, with recent severe el Niños occurring about 14–19 years apart (Ortlieb, 2000; Quinn et al., 1987). Recent very strong el Niños (Multivariate ENSO Index ≥2.0 (Zhang et al., 2019), occurred during the 1972–1973, 1982–1983, 1997–1998, and 2015–2016 austral summers. The last is the only event coinciding with adequately high spatial- and temporal-resolution earth-observation data.

Among ENSO's most significant impacts are inversions in ENSO-neutral precipitation regimes due to Pacific SSTA effects on atmospheric moisture (Fig. 2). During ENSO positive (el Niño) phases, higher elevation Atlantic – Amazonian orographic patterns weaken, decreasing precipitation in mesic - humid regions of the continental interior that feed coastal streams. Conversely, localized precipitation along the Pacific coast of South America increases dramatically (Goldberg et al., 1987; Lavado-Casimiro and Espinoza, 2014; Rau et al., 2017; Tapley and Waylen, 1990). During recent strong – very strong el Niños, EP (ENSO 1 + 2), CP and EP SSTA drove anomalously high amounts of rainfall within the our study region (Cai et al., 2020). Mean precipitation at Casa Grande and San Benito during thermal years 1992–1983, 1997–1998, and 2016–2017 (the last three strongest ENSO-positive phases) was 145 mm/annum and 1905.2 mm/annum, respectively (SENAMHI 2019). ENSO-negative (la Niña) phases are associated with strengthening of ENSO-neutral conditions (Bendix, 2000; Cai et al., 2020; Goldberg et al., 1987; Kane, 1999; Lagos et al., 2008; Lavado-Casimiro and Espinoza,

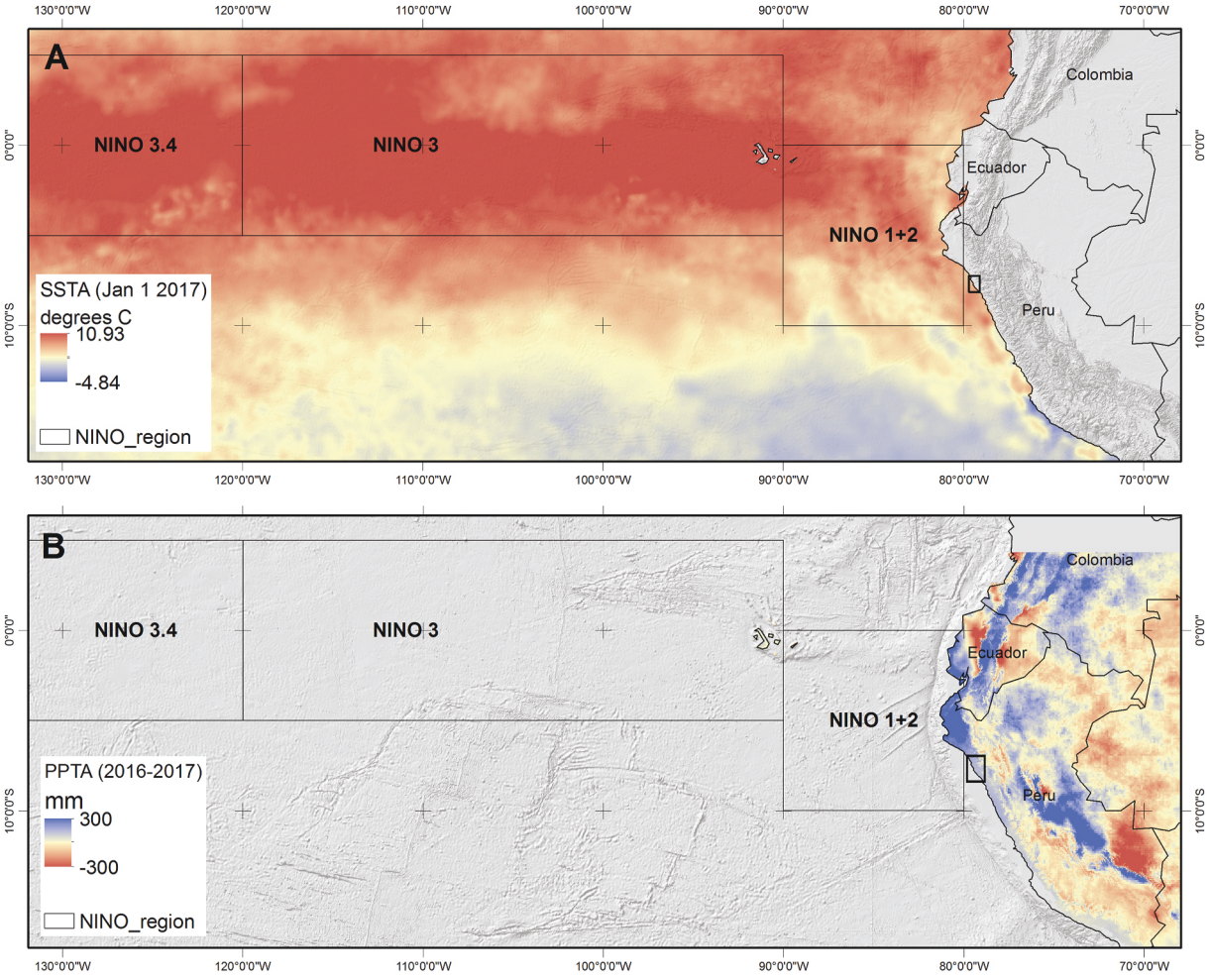

Fig. 2. ENSO regions 1 + 2 and 3.4 sea surface temperature anomalies (SSTA) and total precipitation anomaly (PPTA) during the 2016–2017 ENSO positive period. SSTA derived from NOAA CRW global 5 km monthly data from mean January and January 2017 conditions. PPTA derived from WorldClim mean monthly datasets and GPM-IMERG total monthly precipitation for Jan–May 2017.

2014; Rau et al., 2017; Tapley and Waylen, 1990).

2.3. Ecological effects of ENSO on NW South America

We limit our discussion here to the effects of eastern Pacific (EP) ENSO-positive conditions on arid northwestern South America. The effects of ENSO are particularly acute here as this region is proximate to core areas of ENSO development (Fig. 2). Most attention has emphasized the adverse effects of positive/el Niño phases. Warm NINO 1–4 SSTA and suppression of cold Antarctic currents in NINO1+2 on marine biota during el Niño phases result in a deepening thermocline and decreased nutrient upwelling. This contributes to collapses of cold-adapted benthic, pelagic, and neritic communities and their replacement by cosmopolitan or warm-adapted species (Castilla and Camus, 1992; Chavez et al., 2003; Ñiquen and Bouchon, 2004). Negative terrestrial impacts including mass wasting and river avulsion/flooding that contribute to lost life, property, economic productivity, socio-economic stress, and increased infectious disease have been widely discussed (Garnica, 1997; Martinez-Urtaza et al., 2008; Ward et al., 2014).

These dramatic impacts do not include vegetation responses to ENSO moisture dynamics, which remain poorly understood. These ENSO-vegetation interactions are critical, however, as they affect land surface dynamics and primary productivity, providing a foundation for other ecological responses to ENSO regimes. Botanical surveys in Peru's coastal dry lands following very strong el Niños in 1982–1983 and 1997–1998 documented enhanced herbaceous and woody growth; increased diversity, leafy biomass, and seed production; lengthened growing periods; and expansions of ruderal species (Cano et al., 1999; Dillon and Rundel, 1990; Erdmann et al., 2008; Ferreyra, 1993; Richter, 2005; Richter and Ise, 2005; Tovar et al., 2018). Increased growth cascade through dryland trophic levels, supporting higher trophic level consumers (Erdmann et al., 2008; Richter, 2005). Both increased and decreased green growth are recorded in moist- and dry-tropical forests during ENSO-positive phases due to variations in plant-available moisture (PAW) and insolation rates (Condit et al., 2004; Nagai et al., 2007; Poveda and Salazar, 2004). Vegetation response consequently is not uniform, but is sensitive to edaphic, orographic, and hydrographic variables (Erdmann et al., 2008; Ferreyra, 1993).

3. Methods

We evaluate changing dryland productivity due to ENSO-positive conditions using a multimethod approach. The influence of ENSO on the study area's climate was evaluated as statistical relationships between meteoric precipitation and NINO SSTA indices. We measure vegetation response to increased precipitation during the 2016–2017 EP el Niño using a GPP time series spanning May 2016–July 2018 derived from the European Space Agency's Copernicus Sentinel 2A and 2B high resolution multispectral satellite imagery (Copernicus, 2017). To evaluate the hypotheses that arid regions became ecologically and agriculturally productive during ENSO-positive phases, we compare GPP trends in endemic dry land vegetation to adjacent agricultural areas that were cultivated using various strategies. These are small-scale polyculture, fertigation monoculture (*Saccharum*), and flood-irrigation monoculture (*Oryza*) intermixed with *Saccharum* fertigation (see above). This direct comparison allows us to evaluate whether increased vegetation potential could offset adverse impacts given different productive strategies.

3.1. Analysis of ENSO-driven precipitation in the study region

Statistical relationships between precipitation in the study region and SSTA indices in NINO regions 1 + 2, 3, 3.4, and 4 (Fig. 3) were evaluated using monthly indices downloaded from the National Center for Atmospheric Research (NCAR) climate data portals (Trenberth, 2021). Instrumental records for the Casa Grande and San Benito pluviometric stations were accessed from SENAMHI data repositories using the R package, **senamhiR** (Anderson, 2020). San Benito provides the more complete record spanning 1964–2019. Data gaps of more than 2 weeks out of a one-month period were filled using a normal-ratio estimation method (Linsley et al., 1988) with concurrent SENAMHI precipitation data from the Cospan, Sinsicap, and Monte Grande stations. The resulting fifty-five year record was used to calculate mean monthly and December–February, (DJF) and March–May (MAM) trimester precipitation throughout the austral thermal year (July–June). The DJF and MAM trimesters characterize the austral wet season in Chicama and are important for evaluating ENSO precipitation anomalies. Monthly precipitation accumulations are plotted against NINO SSTA for ENSO-positive periods during 1982–1983, 1997–1998, and 2016–2017 in Fig. 3. Also shown are the average MODIS NDVI for the matorral subregion and a harmonic fitted curve (Shumway and Stoffer 2017) during the most recent ENSO neutral – positive years derived using Google Earth Engine. These plots show the strong relationship between SST warming, precipitation increases, and increased vegetation green growth in the study region.

Statistical relationships between NINO 1 + 2 and 3.4 SSTA reported by NCAR and precipitation recorded at the SENAMHI San Benito station were evaluated using online tools available through the Koninklijk Nederlands Meteorologisch Instituut Climate Explorer (KNMI-CE, Trouet and Van Oldenborgh, 2013) San Benito monthly precipitation totals were uploaded and anomalies were calculated as increases/decreases from monthly means. NINO region 1 + 2 monthly SST anomalies for the period 1964–2019 were similarly uploaded into KNMI-CE. Detrended precipitation anomalies from San Benito from December–May (the wet season) were correlated to detrended NINO 1 + 2 SST anomalies with a 1-month lag to allow SST trends to propagate.

3.2. Estimation of gross primary productivity from optical remote sensing

We quantify the vegetation response to enhanced 2016–2017 el Niño rainfall as gross primary productivity (GPP) rather than use a dimensionless vegetation index. GPP is the amount of energy photochemically stored by plants per unit area per unit time and is a measure of productivity that is critical for estimating Net Primary Productivity (NPP, the amount of biomass available to consumers as plant starches and sugars). However, NPP is a function of autotrophy and stored biomass (including below-ground) rates and cannot be reliably estimated from remotely-sensed data without plant community-specific parameters. In lieu of these parameters for our study region, we rely on estimated GPP to evaluate plant dynamics.

GPP can be readily estimated from remote sensing data as a function of (1) plant photosynthetic activity, (2) amount of incident photosynthetically-active radiation (PAR_{in}) available to plants for photosynthesis, and (3) carbon transfer rates (Running et al., 2000). Canopy-level chlorophyll content is the strongest predictor of photosynthetic activity while accounting for phenology, stress, or species-dependent photosynthetic capacity (Gitelson et al., 2006). Chlorophyll-sensitive vegetation indices (VI_c) and fractional Photosynthetically Active Radiation (fPAR) are the most reliable remote sensing measures of plant photosynthetic activity from which to estimate GPP, consequently (Gitelson et al., 2006; Lin et al., 2019). PAR_{in} is determined by solar incidence and environmental variables including cloud cover and shade (Lin et al., 2019). Dense canopy and/or canopy geometry, which can also affect PAR_{in} diurnally, is not a factor in the study region. Consequently, the most significant factors affecting PAR_{in} are seasonal variations in solar incidence and daily variations in cloud cover. Environmental variables that influence carbon transfer rates, including temperature, atmospheric vapor, and nutrient availability (Running et al., 2000), are nearly constant within the study region, given its coastal/tropical location, the spatial scale of analysis, and elevational range.

Gitelson et al. (2006) calculate GPP from remote sensing data as a function of VI_c and PAR_{in} as:

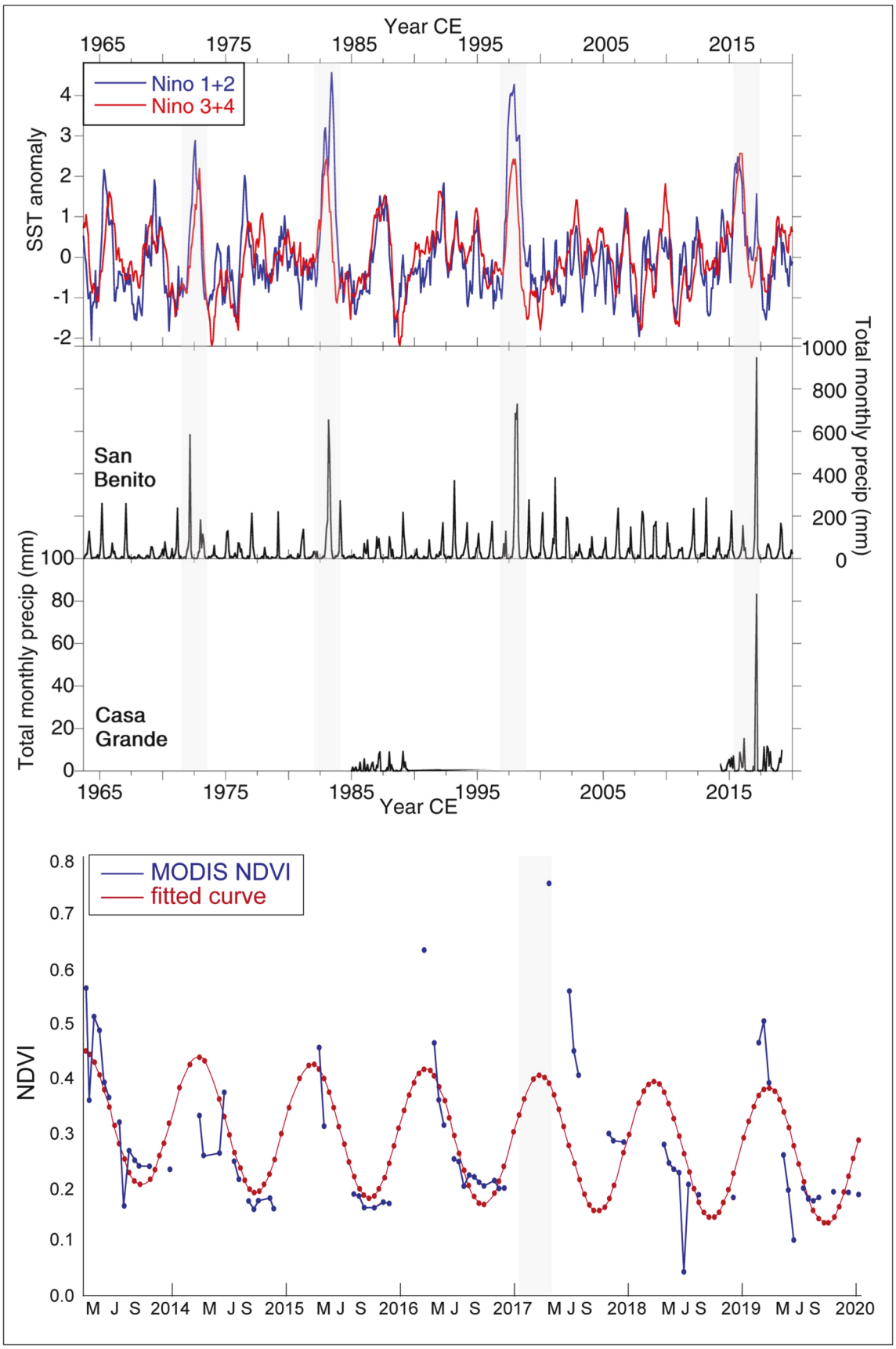

Fig. 3. Time series showing relationships between NINO1+2 and 3.4 SSTA, precipitation in the study region, and vegetation dynamics for the most recent ENSO positive period. ENSO positive periods are shaded grey.

$$GPP \propto VI_c \times PAR_{in} \quad (1)$$

where VI_c

$$VI_c = \frac{\rho_{840—870}}{\rho_{720—740}} - 1 \quad (2)$$

Similarly, Lin et al. (2019) find a close relationship between GPP estimated from Sentinel data and carbon flux tower eddy-covariance measurements of GPP (GPP_{EC}), using the formula

$$GPP \propto CL_r \times PAR_{in} \quad (3)$$

where CL_r is a chlorophyll-sensitive vegetation index similar to VI_c, given as:

$$CL_r = \frac{\rho_{783}}{\rho_{705}} - 1 \quad (4)$$

Correlations between GPP_{EC} and Sentinel GPP estimates were strongest in partially-vegetated grasslands where canopy effects on PAR were minimal (Lin et al., 2019). This is similar to the conditions in our study region.

While carbon transfer rates are relatively constant within phenological stages (active growth and senescence) of short-lived/annual plants, they can vary across phenological stages (Gitelson et al., 2006; Lin et al., 2019; Running et al., 2000). The MODIS MOD17A2 GPP product (Running et al., 2004; Running and Zhao, 2015) controls for this with a seasonally-varying biome-specific light use efficiency factor (LEU, ε) to calculate GPP as

$$GPP = \varepsilon \times (fPAR \times PAR_{in}) \quad (5)$$

Similarly, Lin et al. (2019) modify equation (3) with flux tower eddy-covariance measurements, to

$$GPP_{CLr\ i} = a_i \times CL_{r\ i} \times PAR_{in} + b_i \quad (6)$$

where a_i and b_i are scene-specific slope and intercept coefficients that control for changing phenological conditions.

3.3. Derivation of a sentinel 2 GPP timeseries

We measure GPP from the Sentinel 2 multispectral (S2-MSI) data using a modified form of equation (6) above. S2-MSI level 1C scenes acquired between May 2016 and July 2018 were selected from the Copernicus Open Access Hub (Copernicus, 2017). Sentinel 2 provides optical data in 13 bands at 10 m and 20 m resolution in the visible – NIR spectrum with a 10-day revisit time at the equator (Table 1). Sentinel 2A was launched on June 23, 2015 followed by the Sentinel 2B platform on March 07, 2017. As these platforms were launched just prior to the onset of the 2016–2017 el Niño, they provide the first opportunity to monitor ENSO-vegetation dynamics through full phenological cycles at the high spatial resolution and spectral resolution that Sentinel provides in the Red, Red Edge, and Near Infrared spectra.

Scenes having ≤5% cloud cover are used here. Sea/land surface temperature differentials create frequent low-altitude coastal vapor in the study region and only 17 out of 121 scenes acquired between Jan 01, 2016–Dec 31, 2018 met scene-quality criteria (SM, Table 1). Radiance values were corrected to ground reflectance and haze removed using scene-specific ephemeris parameters and a mid-latitude arid atmospheric model.

We substituted fPAR for the vegetation photosynthesis terms in the equations above to approximate GPP as:

$$GPP_{S2} = a_i \times fPAR_{S2} \times PAR_{in} + b_i \quad (7)$$

Where fractional PAR is calculated following Wiegand et al. (1990), as:

$$fPAR = 1.0 \times (1\text{-}1^{(-0.4 * LAI)}) \quad (8)$$

where leaf area index (LAI) is given as:

$$LAI = (3.618 \times EVI)\text{-}0.118 \quad (9)$$

and enhanced vegetation index (EVI) is given as:

$$EVI = 2.5 \times ((\rho_{783} - \rho_{705}))/(1+\rho_{783}+(6 \times \rho_{705})-(7.5 \times \rho_{492})) \quad (10)$$

Following Lin et al. (2019), S2-MSI bands 7, 5, and 2 are used for ρ_{783}, ρ_{705}, and ρ_{492}, respectively.

Average daily PAR_{in} was derived for each S2-MSI scene date from the MODIS L3 MCD18A2 v006 product (SM, Table 2). MCD18A2 provides daily measurements of PAR in W/m2 at 3 h intervals and 5 km resolution (Wang, 2017). The products for Universal Time Coordinated (UTC) 1200, 1500, 1800, and 2100 (7:00 a.m., 10:00 a.m., 1:00 p.m., and 4:00 p.m. local time) were accessed from the USGS LPDAAC archives and summed to calculate cumulative daily PAR. PAR_{in} was estimated by averaging the daily summed MCD18A2 PAR in seven-day periods bracketing for each S2-MSI scene date for the years 2016–2020, such that estimated PAR_{in} is the average of 28 MCD18A2 tiles. The results are date-specific estimates of mean daily PAR_{in} affected by solar illumination while minimizing cloud cover effects.

Neither flux tower data nor LEU (ε) coefficients are available for the study region. In lieu of these data, we corrected initial GPP_{S2}

Table 1
Sentinel 2A and 2B multispectral instrument band orders, with bandwidth, central frequencies, and nominal spatial resolutions for each band indicated.

Sentinel-2 MSI data	Sentinel-2A		Sentinel-2B		
	Central wavelength (nm)	Bandwidth (nm)	Central wavelength (nm)	Bandwidth (nm)	Spatial resolution (m)
Band 1 - Coastal aerosol	442.7	21	442.2	21	60
Band 2 - Blue	492.4	66	492.1	66	10
Band 3 - Green	559.8	36	559	36	10
Band 4 - Red	664.6	31	664.9	31	10
Band 5 - Vegetation red edge	704.1	15	703.8	16	20
Band 6 - Vegetation red edge	740.5	15	739.1	15	20
Band 7 - Vegetation red edge	782.8	20	779.7	20	20
Band 8 - NIR	832.8	106	832.9	106	10
Band 8A - Narrow NIR	864.7	21	864	22	20
Band 9 - Water vapor	945.1	20	943.2	21	60
Band 10 - SWIR - Cirrus	1373.5	31	1376.9	30	60
Band 11 - SWIR	1613.7	91	1610.4	94	20
Band 12 - SWIR	2202.4	175	2185.7	185	20

MODIS data	Path/row	product	Temporal resolution	Spatial resolution (m)
MOD17A2H	H10/V09	Gross primary productivity (GPP)	8-day average	500
MCD18A2 v006	H10/V09	Ambient photosynthetic radiation (APAR)	Daily (3 h intervals)	5000

Table 2
List of Sentinel 2 A/B scenes and corresponding MODIS MOD17AH2 Gross Primary Productivity products used in this analysis.

scene pair	Sentinel scene	MOD17A2 scene date	image pair corr. pearson ρ	intercept (a)	coefficient (b)	adj. R-squared	f-statistic	df	p-value
1	S2A_GPP_2016_05_02	MOD17A_2016_121	0.816	48.827	0.011	0.6662	4989	2498	<2.2e-16
2	S2A_GPP_2016_08_11	MOD17A_2016_225	0.703	43.670	0.025	0.4934	2435	2498	<2.2e-16
3	S2A_GPP_2016_10_10	MOD17A_2016_281	0.738	47.080	0.007	0.5443	2985	2498	<2.2e-16
4	S2A_GPP_2016_11_10	MOD17A_2016_313	0.762	47.060	0.007	0.5808	3464	2498	<2.2e-16
5	S2A_GPP_2016_11_29	MOD17A_2016_337	0.768	17.330	0.002	0.5892	3586	2498	<2.2e-16
6	S2A_GPP_2017_01_27	MOD17A_2017_025	0.682	40.420	0.001	0.4644	2167	2498	<2.2e-16
7	S2A_GPP_2017_02_16	MOD17A2017_045	0.709	14.640	0.005	0.5027	1910	1888	<2.2e-16
8	S2A_GPP_2017_04_04	MOD17A2017_097	0.790	17.680	0.004	0.6242	3884	2337	<2.2e-16
9	S2A_GPP_2017_04_27	MOD17A2017_113	0.795	37.360	0.004	0.6319	3970	2311	<2.2e-16
10	S2A_GPP_2017_05_17	MOD17A_2017_137	0.785	−33.600	0.002	0.6164	4016	2498	<2.2e-16
11	S2A_GPP_2017_06_06	MOD17A2017_153	0.732	49.990	0.012	0.5361	2368	2047	<2.2e-16
12	S2A_GPP_2017_10_14	MOD17A2017_305	0.727	2.931	0.002	0.5285	2282	2034	<2.2e-16
13	S2A_GPP_2018_02_11	MOD17A_2018_041	0.792	51.620	0.007	0.6263	4190	2498	<2.2e-16
14	S2A_GPP_20180313	MOD17A_2018_073	0.766	37.090	0.008	0.5859	3537	2498	<2.2e-16
15	S2A_GPP_2018_05_02	MOD17A_2018_121	0.824	24.610	0.009	0.6784	5273	2498	<2.2e-16
16	S2A_GPP_2018_05_22	MOD17A_2018_145	0.676	70.610	0.009	0.4564	2099	2498	<2.2e-16
17	S2A_GPP_2018_07_31	MOD17A_2018_209	0.774	40.910	0.021	0.5992	3736	2498	<2.2e-16

measurements by regressing them to a corresponding MODIS 8-day global MOD17A2 GPP product to derive a_i and b_i coefficients as in equations (6) and (7). (MOD17A2 provides 8-day GPP in kg C/day^{-1} with global coverage at 500 m resolution. Because of the MOD17A2 product's lower resolution and use of a biome-level ε variable, it is inappropriate for measuring GPP at this study's localized scale. Correlations between GPP_{S2} and MOD17A2 scene pairs were evaluated using Pearson's ρ (Fig. 4, SM, Table 1). Final GPP_{S2} measurements were derived by regressing the initial estimates against MOD17A2 using a linear model and recalculating GPP as in equation (7).

We assessed temporal trends by measuring GPP at each step in the time series within the six phytogeographic subregions using sets of randomly-generated sampling loci (n = 2500, see SM Table 3–5 for values).

4. Results

Precipitation in the study region is positively correlated with SSTA in the NINO 1 + 2 and NINO 3.4 regions, indicating that significant precipitation such as occurred in 2016–2017 is derived from EP and CP el Niños.

GPP_{S2} measurements are strongly positively correlated with MODIS 8-day global MOD17A2 GPP. GPP_{S2} measurements reveal divergent patterns in GPP between endemic arid land and agricultural vegetation types. All three agricultural subregions exhibit cyclic seasonal increases/decreases in GPP. These patterns are nominally affected by 2016–2017 el Niño. In contrast, endemic dry land vegetation shows a very strong response to anomalous rainfall amounts driven by the 2016–2017 EP el Niño. GPP in two of the three desert communities dramatically increased. Similar responses were not seen in the prior/subsequent ENSO-neutral wet seasons.

4.1. Dynamics of the 2015–2017 very strong Eastern Pacific el niño

Conditions affecting the NW coast of South America from 2015 to 2017 conform to a class of "Eastern Pacific el Niños," where warming occurs in the eastern Pacific (NINO1+2 region) separately from or following central Pacific (NINO 3.4) warming (Cai et al., 2020; Hu et al., 2019). NINO 1 + 2 and 3.4 SSTA indicate the establishment of ENSO-positive conditions between April 2015–April 2016, contributing to marginally enhanced precipitation at Casa Grande and San Benito during the 2016 late austral winter wet season (Fig. 3). NINO 1 + 2 SSTA increased the following austral summer wet season, from December 2016–March 2017 with weaker SSTA in NINO 3.4. While warm/positive SSTA persisted from approximately May 2015–July 2017, strong positive conditions in NINO 1 + 2 from December 2016–2017 catalyzed increased precipitation on the NW coast of South America.

Precipitation accumulation from December 1, 2016–May 30, 2017 totaled 146.6 mm at Casa Grande and 1610.3 mm at San Benito, increases of 683% and 395% over mean annual amounts recorded at the same stations from 1964 to 2020 (Fig. 3). Rainfall began in late January, becoming more frequent and intense through the beginning of April. Single stormy events at Casa Grande exceeded 40 mm of precipitation, whereas total annual precipitation in the three years prior and since was <40 mm. Rainfall subsequently decreased with a return to non-anomalous precipitation after April 2017.

Monthly precipitation totals at San Benito are strongly correlated with NINO1+2 SSTA ($\rho = 0.715$). While precipitation in the study region is positively correlated with NINO3+4 SSTA, these relationships are weaker ($\rho = 0.260$). This is consistent with observations that Andean orographic precipitation primarily is Atlantic-Amazonian in source with little meteoric moisture on the Pacific coastal region, except for when ENSO conditions invert this pattern (Kane, 1999; Lavado-Casimiro and Espinoza, 2014; Rau et al., 2017; Tapley and Waylen, 1990; Vuille et al.,

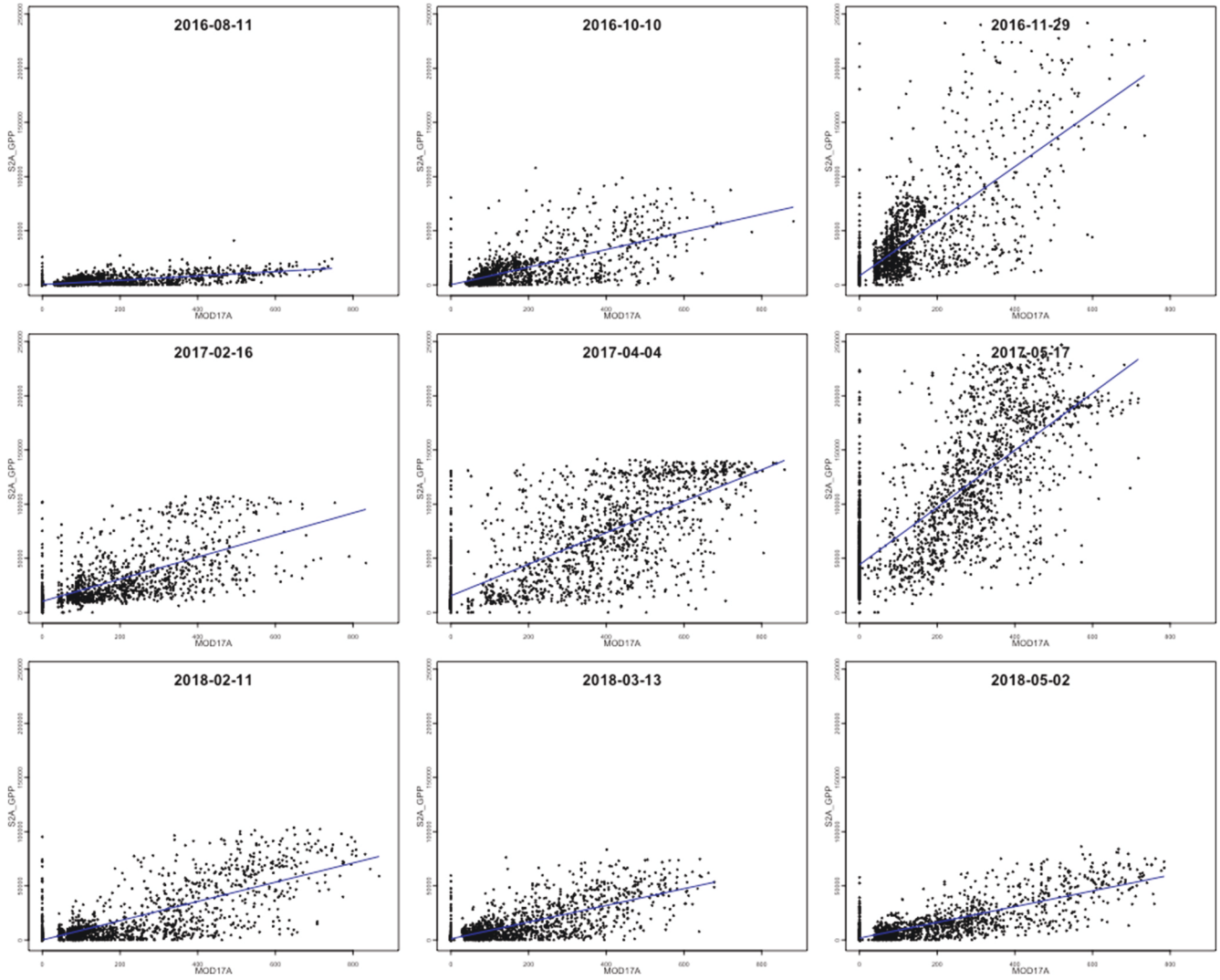

Fig. 4. Scatter plots showing the relationship between MODIS MOD17AH2 GPP measurements and GPP estimated as a product of Sentinel 2 fPAR and average weekly PAR estimated from 2019 to 2020 MODIS MCD18A2 data.

2000). Direct precipitation is most strongly affected by eastern Pacific and eastern equatorial SST warming, as occurred during the 2016–2017 EP el Niño.

4.2. Validation of sentinel 2 GPP measurements

Initial estimates of GPP_{S2} are strongly positively correlated with MODIS GPP ($\rho = 0.676$ to $\rho = 0.824$, see Fig. 4 and Table 2). With this strong positive correlation, GPP can reliably be estimated from S2-MSI fPAR. Weaker correlations occur in scene pairs during the wet seasons. This is likely due to increased spectral heterogeneity from cloud cover and patchy vegetation which is not resolved between the 500 m MODIS and 10 m S2-MSI products. Based on strong correlations, however, linear models using scene-specific a_i and b_i coefficients can be used to derive GPP as in equation (7).

4.3. Responses of vegetation communities to EP el niño source moisture

Vegetation in the studied phytogeographic subregions show variable responses to enhanced ENSO moisture (Fig. 5). Sample values, means, and standard errors for each subregion are provided in the Supplemental Material Tables 5 and 6 and are shown graphically in Fig. 6. Agricultural areas show moderate changes relative to ENSO-neutral wet/dry seasons. Agricultural GPP has regular seasonal variation, as wet season (Dec–May) high elevation precipitation benefits irrigation agriculture along the coast. During the wet season (Figs. 5A and 6), mean GPP_{S2} increases to ~ 160–450 mg C m^2 day^{-1}. Peak productivity occurs in all years towards the end of the wet season (April–May) as cultivars enter maturation stages. Lowest GPP_{S2} occurs after the wet season as cultivated areas enter fallow periods. Mean ENSO neutral dry season GPP_{S2} (Figs. 5B and 6) is ~150–300 mg C m^2 day^{-1}. Two agricultural subregions (*Saccharum/Oryza* monoculture, *Saccharum* monoculture) show modest increases in GPP_{S2} under ENSO positive conditions compared to ENSO neutral years, while the third shows moderate decreases (Fig. 6, and SM, Table 6). While ENSO-related agricultural losses are reported due to lost arable area and infrastructure damages avulsion and slope destabilization, these losses do not appear to be compounded by large fluctuations in GPP.

In contrast to agricultural subregions, the response of endemic desert vegetation to ENSO-driven moisture is dramatic. During ENSO neutral conditions, vegetation growth is extremely limited and the desert regions are effectively denudate (Fig. 5 A and B). Levels of GPP in the lower elevation desert regions are <100 mg C m^2 day^{-1}. The desert matorral phytogeographic region has moderately more vegetation productivity: ENSO neutral GPP averages ~130 ± 2.8 mg C m^2 day^{-1} with slightly higher levels late in the wet season (May).

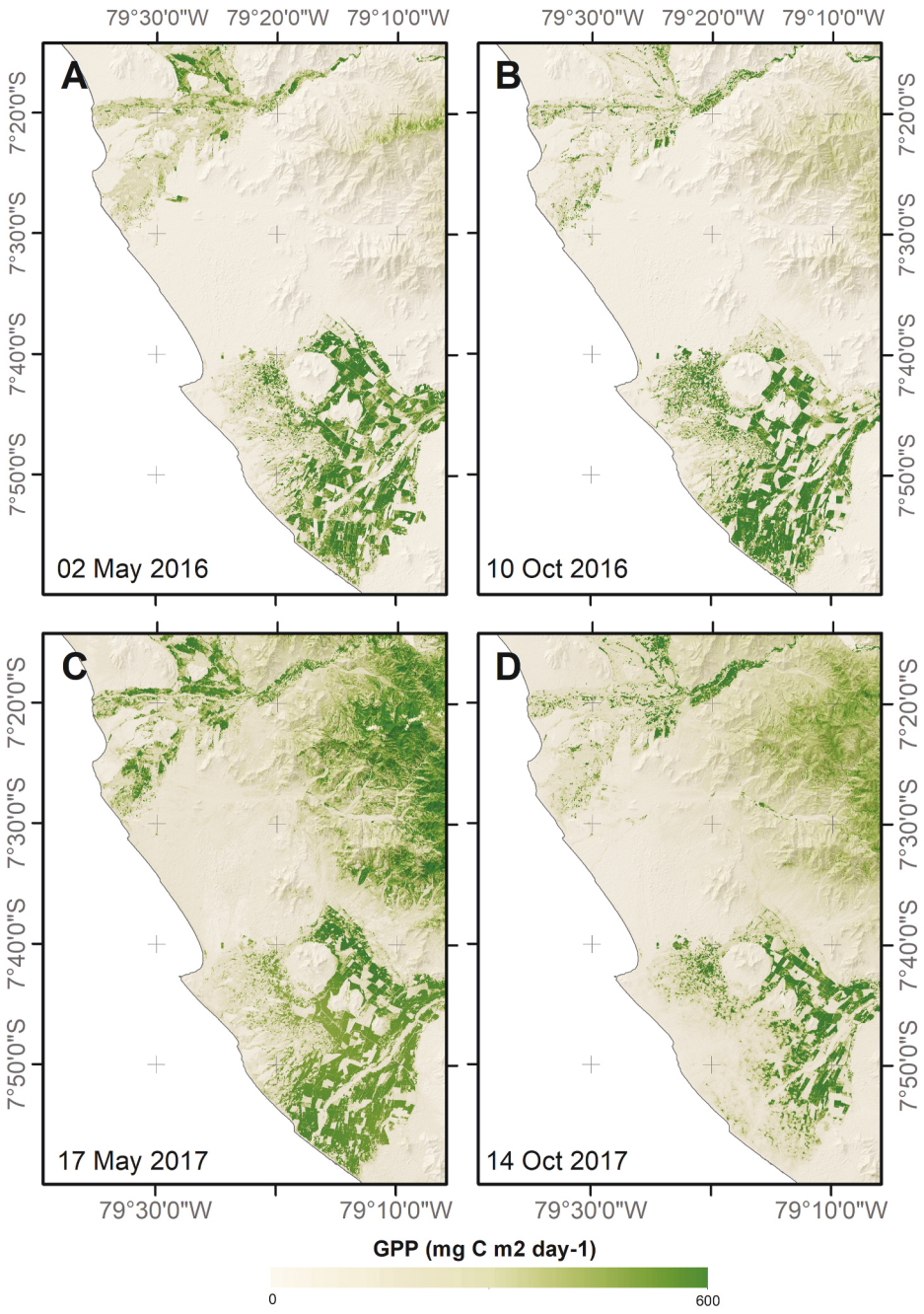

Fig. 5. Gross Primary Productivity derived from Sentinal 2A MSI Level 1C data for ENSO-neutral wet season (May 02, 2016) and dry season (Oct 10, 2016), Compared to ENSO-positive wet season (May 17, 2017) and dry season (October 14, 2017).

Endemic vegetation in the desert piedmont and matorral phytogeographic subregions responded rapidly and significantly to enhanced el Niño moisture during the 2016–2017 wet season (Fig. 5 C and D). Maximal GPP_{S2} in these two regions occurred from early April – mid May 2017, 4–8 weeks after peak precipitation was recorded at Casa Grande and San Benito. Peak GPP_{S2}, measured on April 04, 2017, reaches 276.3 ± 2.8 mg C m^2 day^{-1} and 396.9 ± 5.2 mg C m^2 day^{-1} in the piedmont and matorral phytogeographic subregions, respectively (Fig. 6). These values represent >260% increases over GPP maxima during prior and subsequent ENSO neutral wet seasons. The desert littoral, importantly, does not show a commensurate greening and levels of GPP during the ENSO positive period are within the range of interannual variability throughout the time series. This subregion is not significantly affected by ENSO conditions.

4.4. Comparisons of agricultural and endemic vegetation productivity between ENSO neutral and positive periods

One aspect of debate concerning ENSO impacts is the effect of el Niño periods on the potential productivity of dryland vegetation and non-industrial agriculture, and ultimately the economic effects of these events on non-industrial economies. A comparison of agricultural and endemic phytogeographic subregions through the time series reveals how significantly ENSO positive conditions affect endemic vegetation primary productivity (Fig. 6). GPP in both the piedmont and matorral phytogeographic subregions is below levels of productivity in all agricultural subregions during ENSO neutral conditions. As the 2016–2017 EP el Niño strengthened, the piedmont and matorral subregions reached levels of productivity comparable to GPP in agricultural areas. This

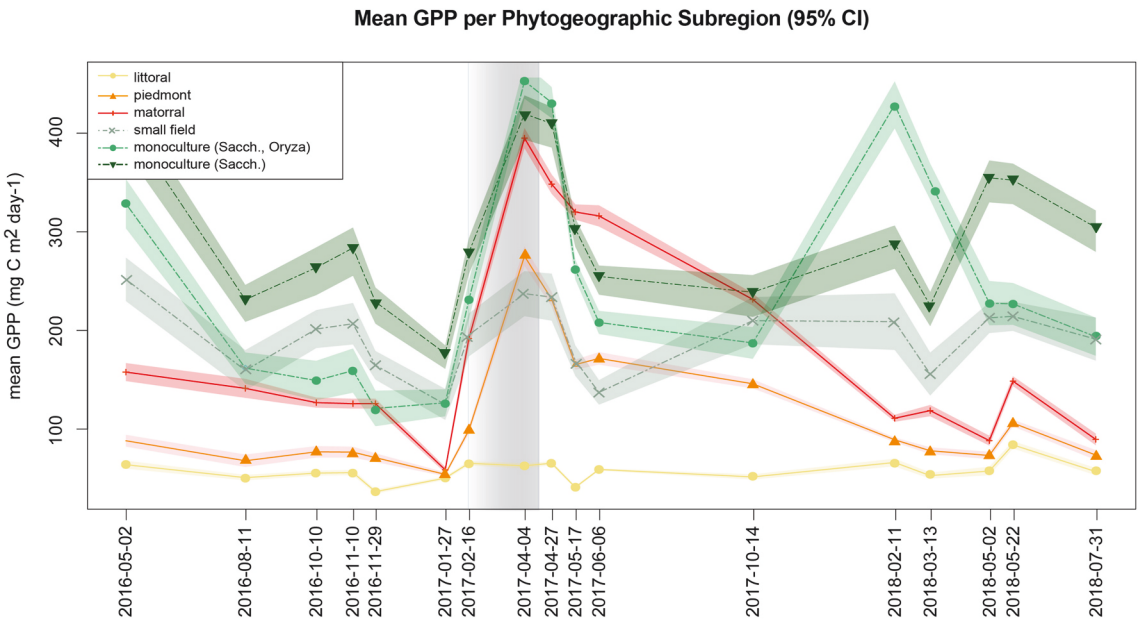

Fig. 6. Time series of GPP_{S2} values showing the mean and 95% confidence interval for six phytogeographic subregions within the study region.

positive response suggests these niches are adapted to respond to ENSO positive conditions and also that agriculturally productive niches could be expanded during these periods.

GPP in the piedmont subregion exceeds small polyculture levels of productivity by early April 2017. Piedmont GPP remains higher than/within the range of small field GPP until at least as late as early Jun 2016. Piedmont GPP drops below agricultural regions sometime after early June 2017 but remains elevated over ENSO neutral levels until as late as October 2017.

The matorral subregion shows the most rapid and dramatic response. By mid-February 2017, mean matorral GPP is comparable to GPP in small-field polyculture plots. By early April (~90 days after substantial ENSO-driven precipitation began), matorral GPP greatly exceeded small polyculture GPP and peaked at levels of productivity commensurate with intensively fertigated *Saccharum/Oryza* monoculture plantations (Fig. 6 and SM Table 6). Matorral GPP remains elevated above ENSO neutral levels until at least as late as Oct 2017 and from mid-May to mid-October of 2017 exceeds or is within the 95% CI of GPP in all three agricultural subregions. Desert matorral GPP exceeds or is equal to small polyculture GPP for a period of minimally 265 days. It exceeds or is within the standard error for *Saccharum/Oryza* monoculture for a period of minimally 204 days. Importantly, the matorral subregion sustained high levels of green growth for longer periods following the 2017 el Niño than did agricultural regions.

The integrals for the piecewise functions defining each phytogeographic subregion further clarify the total effect of ENSO-driven moisture on GPP (Fig. 7). During ENSO neutral periods in this series (May 2016–Jan 2017 and Oct 2017–May 2018), the integrals for piedmont ($\int = 3.5 \times 10^4$) and matorral ($\int = 5.5 \times 10^4$) subregions are 27% and 43%, respectively, of the integral for the most productive agricultural region, *Saccharum* monoculture ($\int = 1.3 \times 10^5$). In response to ENSO positive conditions (Jan–Oct 2017), integrals for the piedmont ($\int = 6.3 \times 10^4$) and matorral ($\int = 1.0 \times 10^5$) subregions approximately double. Cumulative GPP in the piedmont and matorral subregions reaches 52% and 84%, respectively, of *Saccharum* monoculture region ($\int = 1.2 \times 10^5$), the most productive phytogeographic subregion under both ENSO neutral and positive conditions. Notably, the ENSO positive matorral vegetation integral is approximately 121% of that of small polyculture fields ($\int = 8.4 \times 10^4$). The marked and sustained increases in the piedmont and matorral subregions indicate high levels of primary productivity are achievable in endemic communities under suitable ENSO positive conditions. Levels of productivity are comparable to those seen in agricultural areas, and the positive effects of the 2016–2017 el Niño on GPP was sustained for longer periods in endemic communities than in agricultural subregions.

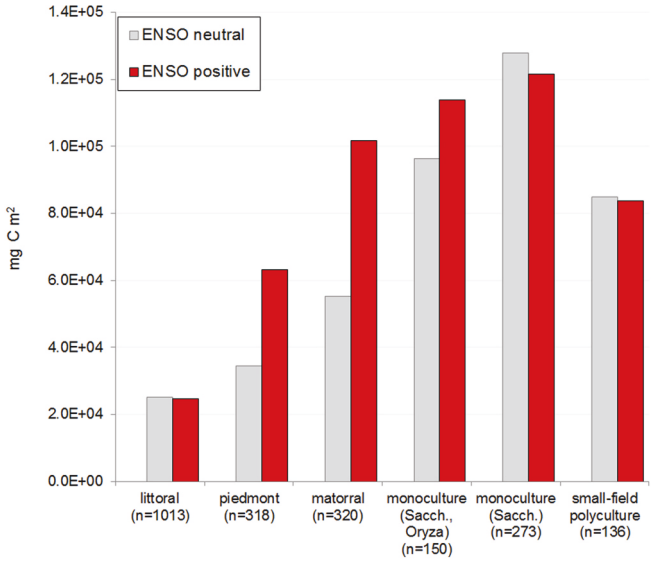

Fig. 7. Integrals for the piecewise functions defining GPP trends in each phytogeographic subregion, during ENSO-neutral and ENSO-positive periods.

5. Discussion

5.1. ENSO effects on arid land vegetation ecology

There is ecological and anthropological debate regarding the effects of ENSO on natural and human systems in NW South American dry lands and how ecological effects of ENSO-positive conditions enabled or limited human adaptation to these abrupt climate changes. Varied responses have been reported for both humid and dry neotropical forests; adverse impacts include decreased leafy biomass due to drier than normal conditions while enhanced green- and sapling growth and

fruiting and seeding have also been recorded (Condit et al., 2004; Nagai et al., 2007; Poveda and Salazar, 2004). However, botanical surveys indicate el Niño events can have a positive effect on—and may be vital to the development and dispersal of—endemic dry land vegetation communities (Cano et al., 1999; Dillon and Rundel, 1990; Eichler and Londoño, 2013; Erdmann et al., 2008; Ferreyra, 1993; Péfaur, 1982; Richter, 2005; Tovar et al., 2018).

We demonstrate that ENSO-derived moisture can increase the GPP of certain dry land vegetation, consistent with hypotheses that ENSO events are critical for the establishment of *lomas* and other endemic communities (see below). Further, ENSO effects on agricultural and endemic vegetation diverge. Two of three endemic vegetation communities exhibited dramatic increases in GPP, while the third and all three agricultural subregions exhibited nominal – no change in GPP from ENSO neutral conditions. Spatial variability in vegetation response is critical to accurately measuring the aggregate ecological effects of ENSO and to understanding how anisotropic conditions result in niche environments that could help mitigate the adverse effects of these climate changes.

5.2. Comparison of results to botanical surveys during prior el niño periods

Botanical surveys following el Niños in 1982–1983, 1997–1998, and 2016–2017 provide fine-grained data on vegetation dynamics apparent as enhanced GPP. Positive or neutral vegetation responses were conditioned by taxa histology and geological substrate. Sentinel 2 measures of GPP improve the spatialization of these relationships, helping to identify the most productive microniches during ENSO positive conditions.

Recorded positive effects include increases in species richness, alpha diversity, and density, with the most pronounced effects observed in herbaceous/perennial Asteraceae, Boraginaceae, Graminaea, Poaceae, Fabaceae, Leguminosae, Solanaceae, and Malvaceae taxa (Cano et al., 1999; Erdmann et al., 2008; Ferreyra, 1993; Richter, 2005; Richter and Ise, 2005; Tovar et al., 2018). Increased green growth was most significant in upland (>500–600 masl) plant communities on well-drained 'pebbly' or 'gravelly' substrates; these conditions correspond to the piedmont and matorral phytogeographic subregions in this study.

Depending on the community, vegetation ground cover increased from 3 to 5% during ENSO neutral conditions to 53–100% of ground cover during prior ENSO positive periods. Greater than 90% of 168 previously-recorded species at Cerro Campana (−7.98°, −79.10°, 1004 masl) were in flower or fruiting between January–October following that year's very strong el Niño; simultaneously, 40 species in *lomas* communities were in flower, compared to only 4 species three years later (Dillon and Rundel, 1990: 495). Vegetation diversity, richness and density in plots in Piura (northern Peru) declined and stabilized within 3 years following the 1997–1998 el Niño, but showed structural changes for up to 6 years (Richter, 2005). Enhanced growth persisted longest in drought-tolerant woody-stemmed herbaceous plants such as *Tephrosia cinerea*, a nitrogenous Fabaceae (Cano et al., 1999; Erdmann et al., 2008; Tovar et al., 2018).

Increases in establishment rates, leafy biomass, and cover (from approximately 1.75%–7.5%) are also recorded in woody species (namely *Prosopis pallid* and *Capparis scabrida* following the 1982–1983 and 1997–1998 el Niños (Erdmann et al., 2008). While the most significant changes in *Prosopis* occurred in the year following ENSO positive conditions, enhanced growth persisted up to six years later, likely due to protracted recharge of phreatic and vadose water (Erdmann et al., 2008).

These structural changes are linked to increased primary productivity in the 9–12 months following the onset of ENSO positive conditions (Fig. 6). Greatly increased GPP can be linked to increased vegetation groundcover in the desert piedmont and matorral phytogeographic regions (Figs. 5 and 6). Enhanced GPP as late as the end of the 2017 calendar year is consistent with botanical surveys that documented increased flowering and green growth up to 10 months following prior el Niño events. We did not record increased productivity into the next wet season/phenological cycles as botanical surveys did following the 1982–1983 and 1997–1998 ENSO positive periods, however. This may be due to more moderate strength of precipitation anomalies during the 2016–2017 EP el Niño and/or to issues of sensor resolution. Importantly, a commensurate increase is not recorded in the littoral regions, suggesting these are not conducive to such a vegetation response.

Increased primary productivity recorded by botanical surveys and remote sensing plays a foundational ecological role. Herbivorous, granivorous, and carnivorous secondary and tertiary consumers also benefit from enhanced vegetation growth following el Niño events. Increased populations of rodents, artiodactyls, reptiles, and raptors were noted during botanical surveys following the 1982–1983 and 1997–1998 ENSO positive periods (Erdmann et al., 2008; Gálvez Mora and Runcio, 2010).

5.3. Implications for human adaptation to ENSO variability

There is some discussion regarding the net ecological effects of ENSO positive periods on human populations. As noted above, most discussion focuses on the adverse impacts on marine and agricultural productivity. Agricultural losses are reported, mostly due to damaged large-scale irrigation infrastructure and lost planting surfaces during floods. However, archaeological and ethnohistorical evidence suggests that the ENSO-positive conditions that benefit endemic vegetation are also sufficient to enable cultivation of areas that are non-arable during ENSO neutral periods (Beresford-Jones et al., 2015; Caramanica et al., 2020; Dillon and Rundel, 1990: 497; Gálvez Mora and Runcio, 2011, 2010).

During the 2016–2017 el Niño, GPP in the matorral region met or exceeded agricultural GPP for periods >200 days, matching and exceeding the growing degree requirements for many cultivars common in the study region. This suggests that enhanced PAW during ENSO-positive phases could meet many growing requirements. Small scale agriculturalists built spring-fed irrigation and garden systems in desert portions of the Chicama Valley following the 1997–1998 el Niño (Gálvez Mora and Runcio, 2010, 2011). Yields were approximately 4500–5000 kg/ha, compared to 5000–6000 kg/ha achievable in valley-floor polyculture plots during ENSO neutral years (Gálvez Mora and Runcio, 2011). Cultivars in these plots included *Brassica* sp., *Cucurbita* sp., *Zea* sp., *Glycine* sp., *Phaseolus* sp., and *Manihot* sp. *Zea* sp. *Zea* sp. and *Triticum* sp. were successfully cultivated on *lomas* near Tacna, Peru after the 1982–1983 el Niño (Dillon and Rundel, 1990: 497). These cultivars require 45 – >240 growing days to reach maturity. Their successful cultivation in normally hyperarid desert environs provides a minimal estimate of how prolonged ENSO effects on groundwater recharge can be. Agriculturalists further capitalized on enhanced green growth during both the 1982–1983 and 1997–1998 el Niños by grazing camelids and caprids on endemic vegetation (Dillon and Rundel, 1990; Gálvez Mora and Runcio, 2011).

The enhanced moisture during ENSO-positive periods and phreatic/vadose groundwater recharge following them expands potential agricultural niches, affording at least the opportunity to partially offset adverse impacts of these abrupt climatic events. A more comprehensive understanding of the ecological transitions which occur during these abrupt climatic changes would consider both the adverse impacts as well as the enhanced potentialities.

6. Conclusions

South America's hyperarid Pacific coastal desert represents one of the largest such biomes globally. Examining the relationships between climatic regimes and vegetation dynamics at a high spatio-temporal resolution is critical for informing our ecological understanding of the region as well as anticipating how ecological dynamics may change with

future climates. Most attention to ENSO effects on South American vegetation has focused on increased/decreased leafy biomass in the humid neotropics. This study presents the only examination of vegetation gross primary productivity in these arid lands through ENSO neutral – ENSO positive periods. It further explicitly spatializes and quantifies variable trends in vegetation GPP vegetation in response to enhanced ENSO moisture. Our results using Sentinel 2 MSI data are positively correlated with MODIS GPP products, demonstrating that S2 can be reliably used to measure GPP at local scales to understand high resolution ecological dynamics in different regions globally. This is a significant methodological advancement. Direct instrumental biophysical measurements, such as those derived from eddy covariance stations, are absent for western South America and cannot be reconstructed for historic events.

During ENSO neutral periods, desert phytogeographic subregions of Chicama are very sparsely vegetated and denudate. These barren landscapes have typically been construed as unproductive and ecologically empty. This changes profoundly under El Niño conditions. Sentinel 2 GPP measures indicate rapid emergence of dormant endemic vegetation in two out of three desert phytogeographic subregions of the Chicama Valley following the 2016–2017 EP el Niño. Crucially, this vegetation fluorescence was not short-lived. Peak GPP was achieved approximately 45 days after the start of ENSO driven precipitation. High levels of GPP were achieved and sustained during development and maturation stages for as much as 240 days. GPP in arid regions reach >300–400 mg C m^2 day^{-1}, more than four times their ENSO-neutral averages. Critically, GPP in the piedmont and matorral phytogeographic regions reached levels commensurate with levels of GPP in intensively-managed agricultural fields during the same period. Hyperarid regions that are sparsely vegetated to denudate under normal ENSO-neutral conditions demonstrate high potentials for productivity during ENSO-positive conditions.

ENSO and longer-term pluvial phases have been hypothesized to be key factors in the formation of endemic fog oases or *lomas* vegetation communities found from tropical – subtropical latitudes on South America's Pacific coast (Cano et al., 1999; Eichler and Londoño, 2013; Tovar et al., 2018). Support for this has come from botanical surveys as well as from archaeological evidence that documents human exploitation of coastal *lomas* environments and currently hyperarid landscapes. Our results are consistent with hypotheses that endemic desert vegetation communities have a rapid and prolonged growth-response to ENSO-positive conditions and that NW South American arid lands may be at least partially adapted to rely on these periodic climatic inversions.

While human usage of these arid environs has been tied to early – mid Holocene pluvial phases (e.g., Chauchat, 1975), more recent studies demonstrate that the utilization of desert environments could have occurred intermittently and been tied to ENSO conditions (Caramanica et al., 2020). The measured increases in GPP in response to the 2016–2017 el Niño are consistent with these models and show that ecologically-productive niches expand dramatically under certain el Niño conditions. ENSO events may support ecologically-critical niches in the ostensibly challenging hyperarid environments of Pacific NW South America. Further, the expansion of ecologically-productive terrestrial regions under ENSO-positive conditions may alleviate some of the adverse impacts of the same el Niño events.

ENSO events are abrupt climate shifts during which novel regimes are briefly established. As anthropogenic climate change warms mean Pacific SST, these regime shifts are predicted to become more frequent and intense (Wang et al., 2019; Yeh et al., 2009). Addressing future climatic changes will require anticipatory strategies based on expanding adaptive capacity. Episodic climatic events like ENSO have the potential to become forecastable using combinations of instrumental, observational, and localized knowledge. Recent el Niños offer opportunities to develop these insights and better understand how this predicted increase in ENSO activity could affect ecological function in one of its core regions of development. This region, like many tropical and economically-developing regions, relies on climate-sensitive agricultural economies. Developing and mobilizing anticipatory adaptive capacity based on a better knowledge of ENSO-driven ecological dynamics, in arid NW South America, including impacts on GPP, can help meet these challenges.

CRediT authorship contribution statement

Benjamin R. Vining: Conceptualization, Methodology, Formal analysis, Writing – original draft, Writing – review & editing, Project administration. **Aubrey Hillman:** Formal analysis, Writing – review & editing. **Daniel A. Contreras:** Visualization, Writing – review & editing.

Declaration of competing interest

The authors declare that they have no known competing financial interests or personal relationships that could have appeared to influence the work reported in this paper.

Acknowledgements

Sentinel 2A and 2B data were accessed through the ESA's Copernicus Data Open Access Hub and through the USGS Land Processes Distributed Active Archive Center (LP DAAC). MODIS data were accessed through the LPDAAC Terra MODIS distribution server. Portions of this research were supported by a National Science Foundation grant (BCS-1848699) to PI Vining. Jason Tullis and Zachary Bradshaw provided very valuable data analytics guidance that made several improvements to this paper possible. David Hillman provided code for data processing.

Appendix A. Supplementary data

Supplementary data to this article can be found online at https://doi.org/10.1016/j.jaridenv.2021.104695.

References

Anderson, C., 2020. senamhiR: A Collection of Functions to Obtain Peruvian Climate Data.
Ashok, K., Behera, S.K., Rao, S.A., Weng, H., Yamagata, T., 2007. El Niño modoki and its possible teleconnection. J. Geophys. Res.: Oceans 112.
Bendix, J., 2000. Precipitation dynamics in Ecuador and northern Peru during the 1991/92 El Nino: a remote sensing perspective. Int. J. Rem. Sens. 21, 533–548.
Beresford-Jones, D., Pullen, A.G., Whaley, O.Q., Moat, J., Chauca, G., Cadwallader, L., Arce, S., Orellana, A., Alarcón, C., Gorriti, M., 2015. Re-evaluating the resource potential of lomas fog oasis environments for Preceramic hunter–gatherers under past ENSO modes on the south coast of Peru. Quat. Sci. Rev. 129, 196–215.
Cai, W., McPhaden, M.J., Grimm, A.M., Rodrigues, R.R., Taschetto, A.S., Garreaud, R.D., Dewitte, B., Poveda, G., Ham, Y.-G., Santoso, A., 2020. Climate impacts of the el Niño–southern oscillation on South America. Nature Reviews Earth & Environment 1, 215–231.
Cano, A.C., Roque, J., Arakaki, M., Arana, C., La Torre, M., Llerena, N., Refulio, N., 1999. Diversidad florística de las Lomas de Lachay (Lima) durante el evento" El Niño 1997-98. Rev. Peru. Biol. 6, 125–132.
Caramanica, A., Mesia, L.H., Morales, C.R., Huckleberry, G., Quilter, J., 2020. El Niño resilience farming on the north coast of Peru. Proc. Natl. Acad. Sci. Unit. States Am. 117, 24127–24137.
Castilla, J.C., Camus, P.A., 1992. The Humboldt-El Niño scenario: coastal benthic resources and anthropogenic influences, with particular reference to the 1982/83 ENSO. S. Afr. J. Mar. Sci. 12, 703–712.
Chattopadhyay, R., Dixit, S.A., Goswami, B., 2019. A modal rendition of ENSO diversity. Sci. Rep. 9, 1–11.
Chauchat, C., 1975. The paijan complex, pampa de Cupisnique, Peru. Ñawpa Pacha: Journal of Andean Archaeology 85–96.
Chavez, F.P., Ryan, J., Lluch-Cota, S.E., Ñiquen, M., 2003. From anchovies to sardines and back: multidecadal change in the Pacific Ocean. Science 299, 217–221.
Condit, R., Aguilar, S., Hernandez, A., Perez, R., Lao, S., Angehr, G., Hubbell, S.P., Foster, R.B., 2004. Tropical forest dynamics across a rainfall gradient and the impact of an El Nino dry season. J. Trop. Ecol. 20, 51–72.
Copernicus, 2017. Sentinel 2A MultiSpectral Instrument Level 1C Data. European Space Agency retrieved from Copernicus Open Access Hub.
Dillon, M.O., Rundel, P.W., 1990. In: The Botanical Response of the Atacama and Peruvian Desert Floras to the 1982-83 El Niño Event. Elsevier Oceanography Series. Elsevier, pp. 487–504.

Eichler, T.P., Londoño, A.C., 2013. ENSO impacts on lomas formation in South Coastal Peru: implications for the pliocene? Adv. Meteorol. 2013.
Erdmann, W., Schulz, N., Richter, M., Rodriguez, E.F., 2008. Efectos del fenómeno del Nino 1997–1998 en la vegetación del desierto de Sechura. Región Paita hasta el ano 2008. Arnaldoa 15, 63–86.
Ferreyra, R., 1993. Registros de la vegetación en la costa peruana en relación con el fenómeno El Niño. Bull. Inst. fr. etudes andines 22, 259–266.
Gálvez Mora, C., Runcio, M.A., 2011. Eventos ENOS (El Niño, La Oscilación del Sur) y el cultivo de maíz en el desierto del sector medio del valle de Chicama, Perú. Archaeobios 5, 147–150.
Gálvez Mora, C., Runcio, M.A., 2010. Eventos ENOS (El Niño, la Oscilación del Sur) y ocupación del desierto entre el Horizonte Temprano y el Intermedio Tardío: análisis de casos en los sectores medios de los valles de Moche y Chicama. Perú. Archaeobios 4.
Garnica, L., 1997. Evaluación ambiental del fenómeno" El Niño 1997-98" en el sector agrario. Rev. Peru. Biol. 6, 180–182.
Gitelson, A.A., Viña, A., Verma, S.B., Rundquist, D.C., Arkebauer, T.J., Keydan, G., Leavitt, B., Ciganda, V., Burba, G.G., Suyker, A.E., 2006. Relationship between gross primary production and chlorophyll content in crops: implications for the synoptic monitoring of vegetation productivity. J. Geophys. Res.: Atmosphere 111.
Goldberg, R.A., Tisnado, M., Scofield, R.A., 1987. Characteristics of extreme rainfall events in Northwestern Peru during the 1982–1983 El Nino period. J. Geophys. Res.: Oceans 92, 14225–14241.
Hu, Z.-Z., Huang, B., Zhu, J., Kumar, A., McPhaden, M.J., 2019. On the variety of coastal El Niño events. Clim. Dynam. 52, 7537–7552.
Kane, R.P., 1999. Rainfall extremes in some selected parts of Central and South America: ENSO and other relationships reexamined. Int. J. Climatol.: A Journal of the Royal Meteorological Society 19, 423–455.
Kluger, L.C., Kochalski, S., Aguirre-Velarde, A., Vivar, I., Wolff, M., 2018. Coping with abrupt environmental change: the impact of the coastal El Niño 2017 on artisanal fisheries and mariculture in North Peru. ICES (Int. Counc. Explor. Sea) J. Mar. Sci. 76, 1122–1130.
Lagos, P., Silva, Y., Nickl, E., Mosquera, K., 2008. El Niño? Related Precipitation Variability in Perú.
Lavado-Casimiro, W., Espinoza, J.C., 2014. Impactos de El Niño y La Niña en las lluvias del Perú (1965-2007). Revista Brasileira de Meteorologia 29, 171–182.
Lin, S., Li, J., Liu, Q., Li, L., Zhao, J., Yu, W., 2019. Evaluating the effectiveness of using vegetation indices based on red-edge reflectance from sentinel-2 to estimate gross primary productivity. Rem. Sens. 11, 1303.
Linsley Jr., R.K., Kohler, M.A., Paulhus, J.L., 1988. Hydrology for Engineers. McGraw-Hill.
Martinez-Urtaza, J., Huapaya, B., Gavilan, R.G., Blanco-Abad, V., Ansede-Bermejo, J., Cadarso-Suarez, C., Figueiras, A., Trinanes, J., 2008. Emergence of asiatic Vibrio diseases in south America in phase with el Niño. Epidemiology 19, 829–837.
Moat, J., Orellana-Garcia, A., Tovar, C., Arakaki, M., Arana, C., Cano, A., Faundez, L., Gardner, M., Hechenleitner, P., Hepp, J., 2021. Seeing through the clouds–Mapping desert fog oasis ecosystems using 20 years of MODIS imagery over Peru and Chile. Int. J. Appl. Earth Obs. Geoinf. 103, 102468.
Nagai, S., Ichii, K., Morimoto, H., 2007. Interannual variations in vegetation activities and climate variability caused by ENSO in tropical rainforests. Int. J. Rem. Sens. 28, 1285–1297.
Ñiquen, M., Bouchon, M., 2004. Impact of El Niño events on pelagic fisheries in Peruvian waters. Deep Sea Res. Part II Top. Stud. Oceanogr. 51, 563–574.
Onern, 1973. Inventario, Evaluacion y Uso Rational de los Recursos Naturalies de la Costa: Cuenca del Rio Chicama. Oficina Nacional de Evaluacion de Recursos Naturales, Lima, Peru.
Ortlieb, L., 2000. The documented historical record of El Nino events in Peru: an update of the Quinn record (sixteenth through nineteenth centuries). El Niño and the Southern Oscillation: Multiscale variability and global and regional impacts 207–295.
Péfaur, J.E., 1982. Dynamics of plant communities in the lomas of southern Peru. Vegetatio 49, 163–171.
Poveda, G., Salazar, L.F., 2004. Annual and interannual (ENSO) variability of spatial scaling properties of a vegetation index (NDVI) in Amazonia. Rem. Sens. Environ. 93, 391–401.
Quinn, W.H., Neal, V.T., Antunez de Mayolo, S.E., 1987. El Niño occurrences over the past four and a half centuries. J. Geophys. Res.: Oceans 92, 14449–14461.
Ramírez, I.J., Briones, F., 2017. Understanding the El Niño costero of 2017: the definition problem and challenges of climate forecasting and disaster responses. International Journal of Disaster Risk Science 8, 489–492.
Rau, P., Bourrel, L., Labat, D., Melo, P., Dewitte, B., Frappart, F., Lavado, W., Felipe, O., 2017. Regionalization of rainfall over the Peruvian Pacific slope and coast. Int. J. Climatol. 37, 143–158.
Richter, M., 2005. Vegetation development before, during, and after el Niño 1997/98 in northwestern perú. Lyonia 8 (2), 2005-Dry Forest Biodiversity and Conservation 1: Biodiversity.
Richter, M., Ise, M., 2005. Monitoring Plant Development after el Niño 1997/98 in Northwestern Perú (Dauerbeobachtung der Pflanzenentwicklung nach El Niño 1997/98 in Nordwest-Peru). Erdkunde 136–155.
Running, S.W., Nemani, R.R., Heinsch, F.A., Zhao, M., Reeves, M., Hashimoto, H., 2004. A continuous satellite-derived measure of global terrestrial primary production. Bioscience 54, 547–560.
Running, S.W., Thornton, P.E., Nemani, R., Glassy, J.M., 2000. Global terrestrial gross and net primary productivity from the Earth Observing System. In: Methods in Ecosystem Science. Springer, pp. 44–57.
Running, S.W., Zhao, M., 2015. Daily GPP and annual NPP (MOD17A2/A3) products NASA Earth Observing System MODIS land algorithm. MOD17 User's Guide 2015.
Senamhi, 2019. Datos Hidrometeorológicos. Servicio Nacional de Meteorologia e Hidrologia, Lima, Peru.
Tapley, T.D., Waylen, P.R., 1990. Spatial variability of annual precipitation and ENSO events in western Peru. Hydrol. Sci. J. 35, 429–446.
Tovar, C., Infantas, E.S., Roth, V.T., 2018. Plant community dynamics of lomas fog oasis of Central Peru after the extreme precipitation caused by the 1997-98 El Niño event. PLoS One 13, e0190572.
Trenberth, K., 2021. NINO SST indices (NINO 1+2, 3, 3.4, 4; ONI and tni) [WWW Document]. The Climate Data Guide: Nino SST Indices (Nino 1+2, 3, 3.4, 4; ONI and TNI). URL. https://climatedataguide.ucar.edu/climate-data/nino-sst-indices-nino-12-3-34-4-oni-and-tni. (Accessed 3 December 2021).
Trouet, V., Van Oldenborgh, G.J., 2013. KNMI Climate Explorer: a web-based research tool for high-resolution paleoclimatology. Tree-Ring Res. 69, 3–13.
Vuille, M., Bradley, Raymond S., Frank, Keimig, 2000. Interannual climate variability in the Central Andes and its relation to tropical Pacific and Atlantic forcing. J. Geophys. Res.: Atmosphere 105, 12447–12460.
Wang, B., Luo, X., Yang, Y.-M., Sun, W., Cane, M.A., Cai, W., Yeh, S.-W., Liu, J., 2019. Historical change of El Niño properties sheds light on future changes of extreme El Niño. Proc. Natl. Acad. Sci. Unit. States Am. 116, 22512–22517.
Wang, D., 2017. MODIS/Terra+Aqua photosynthetically active radiation daily/3-hour L3 global 5km SIN grid V006 [Data set]. NASA EOSDIS Land Processes DAAC.
Ward, P.J., Jongman, B., Kummu, M., Dettinger, M.D., Weiland, F.C.S., Winsemius, H.C., 2014. Strong influence of El Niño Southern Oscillation on flood risk around the world. Proc. Natl. Acad. Sci. Unit. States Am. 111, 15659–15664.
Wiegand, C., Gerbermann, A., Gallo, K., Blad, B., Dusek, D., 1990. Multisite analyses of spectral-biophysical data for corn. Rem. Sens. Environ. 33, 1–16.
Yeh, S.-W., Kug, J.-S., Dewitte, B., Kwon, M.-H., Kirtman, B.P., Jin, F.-F., 2009. El Niño in a changing climate. Nature 461, 511.
Zhang, T., Hoell, A., Perlwitz, J., Eischeid, J., Murray, D., Hoerling, M., Hamill, T.M., 2019. Towards probabilistic multivariate ENSO monitoring. Geophys. Res. Lett. 46, 10532–10540.